# Thermodynamics of the Unfolding and Spectroscopic Properties of the V66W Mutant of *Staphylococcal* Nuclease and Its 1−136 Fragment†

Maurice R. Eftink,*,‡ Roxana Ionescu,‡ Glen D. Ramsay,‡,§ Cing-Yuen Wong,‡ Jie Q. Wu,|| and August H. Maki||

*Department of Chemistry, University of Mississippi, University, Mississippi 38677, and Department of Chemistry, University of California-Davis, Davis, California 95616*

*Received December 19, 1995; Revised Manuscript Received April 15, 1996*⊗

ABSTRACT: Spectroscopic studies have been performed to characterize the solution structure of the V66W mutant of *Staphylococcal* nuclease and the corresponding 1−136 fragment, referred to as V66W′. Whereas wild-type nuclease has a single tryptophan residue at position 140, the V66W mutant has a second tryptophan residue at position 66, which is the only such residue in V66W′. Steady-state and time-resolved fluorescence studies show Trp-66 in V66W′ to have a blue emission, a relatively large fluorescence quantum yield, a long lifetime, a significant degree of protection from solute quenchers, and to depolarize with a relatively long rotational correlation time. These results characterize Trp-66 in V66W′ as being a buried residue, which indicates that this fragment retains some global structure. Circular dichroism (CD) data are consistent with the fragment having lost most of the α-helical content of the wild type, while retaining $\beta$-sheet structure. The CD spectrum in the aromatic region also suggests that Trp-66 in the fragment experiences an asymmetric environment, which is not identical to that in the full length mutant, V66W. In addition, optical detection of triplet state magnetic resonance (ODMR) spectroscopy can clearly resolve the tryptophan residues and demonstrates differences between the local environment of Trp-66 in V66W and in V66W′, as well as small differences in the Trp-140 environment in wild type and in V66W. Guanidine-HCl induced and thermally induced unfolding studies were performed by simultaneously acquiring CD and fluorescence data as a function of the perturbation and then performing a global analysis of such multiple data sets in terms of two-state and three-state unfolding models. Whereas data for wild-type nuclease and the V66W′ fragment are well characterized by a two-state unfolding model, data for the V66W mutant are better characterized by a three-state process. That is, both the denaturant- and temperature-induced unfolding of V66W involves the significant population of an equilibrium unfolding intermediate. Our global analyses yield thermodynamic parameters for the unfolding transitions, and we show that the data for V66W can be described by a constrained three-state model in which the transition of the intermediate to the fully unfolded state is fixed to have the same thermodynamic parameters that describe the unfolding of the V66W′ fragment.

Nuclease A from *Staphylococcus aureus* has been extensively investigated with regard to its structure and the thermodynamics and kinetics of its folding (Anfinsen et al., 1971; Shortle & Meeker, 1986; Shortle et al., 1990; Loll & Lattman, 1989; Alexandrescu et al., 1990; Evans et al., 1989; Sugawara et al., 1991; Flanagan et al., 1993; Fink et al., 1993; Carra et al., 1994a). Among the large number of mutants that have been studied, V66W[1] has proved an interesting case (Gittis et al., 1993; Carra et al., 1994). V66W has a second fluorescent tryptophan residue in the $\beta$-barrel N-terminal half of the protein. The single tryptophan in the wild type, Trp-140, is at the end of the C-terminal α-helix. V66W thus has two fluorescent reporter groups in what can be considered to be two subdomains of the protein.

An interesting feature of V66W is that it deviates from the two-state unfolding model when subjected to guanidine-HCl induced unfolding (Gittis et al., 1993). Whereas wild-type nuclease shows two-state guanidine unfolding (as demonstrated by similar unfolding profiles for fluorescence and circular dichroism signals), the V66W mutant shows a guanidine unfolding transition curve that requires a three-state unfolding model. Thermal unfolding studies with V66W, using differential scanning calorimetry (DSC), have also shown it to be a three-state process (Carra et al., 1994).

In studying the guanidine induced unfolding of V66W, Gittis and co-workers also prepared a 1−136 fragment,

† This research was supported by NSF Grant MCB 9407167 to M.R.E. and NIH Grant ES 02622 to A.H.M.

* To whom to address correspondence.
‡ University of Mississippi.
§ Present address: Aviv Associates, Lakewood, NJ 08701.
|| University of California−Davis.

⊗ Abstract published in *Advance ACS Abstracts,* June 1, 1996.

[1] Abbreviations: $\alpha_i$, pre-exponential factors of fluorescence intensity decay for component *i*; ANS, 1-anilinonaphthalene-8-sulfonic acid; CD, circular dichroism; $\Delta C_p$, heat capacity change for unfolding transition; DSC, differential scanning calorimetry; $F_o$ and $F$, fluorescence intensity, in the absence and presence of solute quencher; $\Delta G°_{o,un}$ and $\Delta G°_{un}$, the standard free energy change for denaturant induced unfolding; $\Delta H°_{m,un}$, the enthalpy change for thermal unfolding; $K_{sv}$, Stern−Volmer dynamic quenching constant; $k_q$, bimolecular quenching rate constant; $m$, dependence of $\Delta G°_{un}$ on denaturant concentration; ODMR, optically detected magnetic resonance; $\phi_1$ and $\phi_2$, the rotational correlation times for global and internal motion of the protein and tryptophan residue; Q, solute quencher; $r_o g_i$, amplitude of anisotropy decay associated with depolarizing motion described by $\phi_i$; $T_m$, thermal transition temperature; $\tau_i$, fluorescence lifetime of component *i*; $\langle\tau\rangle$, mean fluorescence lifetime, $= \sum\alpha_i\tau_i$; $V$, static quenching constant; V66W, mutant of nuclease having valine at position 66 substituted by tryptophan; V66W′, 1−136 fragment of V66W (also referred to as Δ137−149 fragment); WT; wild type *Staphylococcal* nuclease A; $\chi^2$, chi squared, goodness-of-fit parameter; $Y_i$, generalized spectroscopic signal for state *i*.

S0006-2960(95)03009-1 CCC: $12.00 

referred to as V66W′. This fragment contains Trp-66, but not Trp-140. The V66W′ fragment shows guanidine-induced unfolding, as monitored by changes in its fluorescence or CD signal, but the stability of this fragment is greatly reduced. Similar 1−136 fragments (but not containing a tryptophan reporter group at position 66) have been studied by Shortle and Meeker (1989) and Flanagan et al. (1992, 1993) using CD, gel filtration, and small angle X-ray scattering (SAXS). These studies show the wild-type 1−136 fragment to be a partially unfolded or expanded state, as compared to the full length protein.

Here we present additional data to characterize the guanidine-induced and thermal unfolding of the V66W mutant and the V66W′ 1−136 fragment. We have used our recently described multidimensional spectrophotometer to track the unfolding transition by simultaneously monitoring CD and fluorescence signals (Ramsay & Eftink, 1994a,b; Ramsay et al., 1995); these data sets are then subjected to weighted nonlinear least-squares analysis to obtain thermodynamic parameters. We also present data on the spectral properties of the Trp-66 residue. Using steady-state and time-resolved fluorescence methods, we will show that Trp-66 of the V66W′ fragment has an unexpectedly blue emission and a long fluorescence lifetime, is relatively protected from solute quenchers, and has a significant degree of independent rotational freedom. Also we will show that the addition of $Ca^{+2}$ and the ligand 3′,5′-bisphospho-2′-deoxythymidine diminishes the rotational freedom of this tryptophan residue.

## MATERIALS AND METHODS

*Materials*. Plasmids containing the gene for nuclease A, V66W, and V66W′ were obtained from Dr. Wesley Stites, University of Arkansas. The plasmids were included into *Escherichia coli*, and the proteins were produced and purified using the procedure of Shortle and Meeker (1989). The purity (estimated to be >95%) of the samples was checked by denaturing electrophoresis. The samples were dissolved into 0.1 M NaCl, 0.01 M tris-HCl, pH 7, or 0.05 M Pipes, pH 7, buffer. Ultrapure guanidine-HCl was obtained from USB Chemicals. Protein concentration was calculated using molar extinction coefficients of $15.6 \times 10^3$ $M^{-1}$ $cm^{-1}$ for WT and V66W′ and $21.1 \times 10^3$ $M^{-1}$ $cm^{-1}$ for V66W at 280 nm. Low temperature ODMR and phosphorescence measurements were made on proteins dissolved in 20 mM pH 7 phosphate buffer containing 0.1 M NaCl. Ethylene glycol was added (33% v/v) as a cosolvent, and the final protein concentration was about 1 mM.

*Methods*. Circular dichroism spectra were taken with an Aviv 62 DS spectropolarimeter (Aviv Associates, Lakewood, NJ) using a 1 cm path length between 260 and 320 nm and a 0.02 cm path length between 180 and 270 nm. Protein concentrations were 20−26 $\mu$M (for both the spectral measurements and the unfolding studies described below). Data were taken at 1 nm intervals (0.6 nm resolution) with integration times of 6 s for the aromatic region and 2 s for the far-UV region; spectra shown in Figure 2 are the average of three runs. Measurements were made at 20 °C, using a thermoelectric cell holder. CD spectra are given as mean residue ellipticities, using a mean residue weight of 114 per amino acid residue (149 residues for WT and V66W; 136 residues for V66W′). CD spectra were analyzed for fractional secondary structure composition (α-helix, $\beta$-sheet, $\beta$-turns, and other) using the SELCON program of Sreerama and Woody (1993).

The guanidine-induced unfolding transitions were obtained using a multidimensional spectrophotometer described elsewhere (Ramsay & Eftink, 1994a; Ramsay et al., 1995). Briefly, this instrument is an Aviv 62 DS spectropolarimeter that has been modified to have a right angle photomultiplier (for fluorescence measurements), a thermoelectric cell holder, and a computer-controlled syringe pump (for addition of denaturant). Software has been written to control the near-simultaneous acquisition of CD and fluorescence data as denaturant is added stepwise. For each signal, the standard deviation is recorded, to enable proper weighting of the different data types in a global analysis. The multiple data sets, along with these standard deviations, were analyzed in terms of two-state or three-state unfolding models (see below) using NONLIN (Johnson & Fraiser, 1985).

Fluorescence lifetime and anisotropy decay data were obtained using an ISS multifrequency phase modulation fluorometer, equipped with an Innova 200 argon ion laser with output at 300 nm. Raw phase and modulation data as a function of modulation frequency were analyzed as described elsewhere to obtain fluorescence decay times (Eftink et al., 1991b). The data were fitted by a multi-exponential decay law

$$I(t) = I_o \sum \alpha_i \exp(-t/\tau_i) \qquad (1)$$

where $\alpha_i$ is the amplitude associated with decay time $\tau_i$. Likewise, differential polarized phase and modulation data were analyzed to obtain rotational correlation times with the following decay law

$$r(t) = \sum r_o g_i \exp(-t/\phi_i) \qquad (2)$$

where $r_o g_i$ is the amplitude associated with rotational correlation time $\phi_i$.

Steady-state fluorescence and solute quenching experiments were performed at 20 °C using a Perkin-Elmer MPF 44A fluorometer. Aliquots of 8 M acrylamide (recrystallized from ethyl acetate) were added to a protein solution, and the fluorescence signal (excitation at 295 nm, emission at 340 nm) was corrected for dilution and absorptive screening as described elsewhere (Eftink & Ghiron, 1981). In experiments with iodide as quencher, protein was added to either a solution containing 0.5 M KI or 0.5 M KCl. Using the method of Job, various portions of these solutions were mixed and the fluorescence signals were measured. Fluorescence quenching data were fitted by the modified Stern−Volmer equation

$$F_o/F = (1 + K_{sv}[Q]) \exp(V[Q]) \qquad (3)$$

where $F_o$ and $F$ are the fluorescence intensities in the absence and presence of quencher, Q, $K_{sv}$ is the dynamic quenching constant, and $V$ is the static quenching constant. For iodide quenching, the Stern−Volmer plots were linear or curved slightly downward. In such cases, eq 3 was fitted with $V = 0$ to obtain $K_{sv}$. For acrylamide quenching, the Stern−Volmer plots were upward curving and were fitted with eq 3, using a nonlinear least-squares program to obtain $K_{sv}$ and $V$, the sum of which was taken to be equal to the effective quenching constant, $K_{sv,eff}$. The apparent quenching rate

constant, $k_q$, was calculated as $K_{sv}/\langle\tau\rangle$ (or $K_{sv,eff}/\langle\tau\rangle$), where the mean fluorescence lifetime, $\langle\tau\rangle$, is equal to $\sum\alpha_i\tau_i$.

Steady-state optically detected magnetic resonance (ODMR) measurements were made on each sample in a liquid He cryostat by monitoring the phosphorescence emission at the 0,0-band peak using a bandwidth of 3 nm. The sample temperature was maintained at 1.2 K by pumping on the liquid He. Signal averaging was carried out with the aid of an A/D board contained in an IBM-compatible 486 computer. The ODMR transitions were fitted to Gaussian line shapes using a nonlinear least-squares fitting program based on the Runge−Kutta method. The results were compared with those obtained from analogous programs provided in Sigma Plot and were found to be identical. Peak frequencies of the tryptophan D-E and 2E transitions were estimated by nonlinear extrapolation of the observed peaks to zero sweep rate using an algorithm developed to account for fast passage effects (Wu et al., 1995). Line widths were taken as those measured at the smallest sweep rate employed (ca. 30 MHz/s). Wavelength-selected ODMR was carried out using a smaller bandwidth of ca. 1 nm. The ODMR equipment and methods have been described previously (Maki, 1984).

*Models for the Unfolding Transitions*. For two-state transition between a native, N, and unfolded, U, state, the following relationships describe the equilibrium constant, $K_{un}$, the partition function, $Q$, and the mole fraction of each state, $X_i$.

$$K_{un} = [U]/[N] \tag{4}$$

$$Q = 1 + K_{un}; \qquad X_N = 1/Q; \qquad X_U = K_{un}/Q \tag{5}$$

The average signal (i.e., CD or fluorescence), $Y$, is given by

$$Y = \sum X_i(Y_i + [d]\delta Y_i/\delta[d]) \tag{6}$$

where $Y_i$ is the intrinsic signal of state i in the absence of denaturant, and $\delta Y_i/\delta[d]$ is the dependence of the signal of each pure state on the concentration of denaturant, $[d]$ (i.e., the baseline slope).

The guanidine-induced unfolding transitions are assumed to be described by the linear free energy relationship

$$\Delta G^\circ_{un} = \Delta G^\circ_{o,un} - m[d] \tag{7}$$

where $\Delta G^\circ_{un} = -RT \ln K_{un}$ is the free energy change for unfolding as a function of denaturant concentration, $\Delta G^\circ_{o,un}$ is the free energy change for the unfolding transition at $[d] = 0$, and $m$ describes the dependence of the free energy change on denaturant concentration. We fitted eqs 4−7 to $Y$ vs $[d]$ data using the nonlinear least-squares program NONLIN (Johnson & Fraiser, 1985).

For thermal unfolding transitions, the average signal as a function of temperature, $T$, is given by

$$Y = \sum X_i(Y_i + T\delta Y_i/\delta T) \tag{8}$$

where $\delta Y_i/\delta T$ is the temperature dependence of the signal for the pure states (assumed to be linear). The $Y$ vs $T$ data were fitted to a two-state model using the following relationship for the free energy change as a function of temperature.

$$\Delta G^\circ_{un} = \Delta H^\circ_{m,un}(1 - T/T_m) - \Delta C_p[T_m - T + T\ln(T/T_m)] \tag{9}$$

In this equation $\Delta H^\circ_{m,un}$ is the enthalpy change for the transition at the transition temperature, $T_m$ ($= \Delta H^\circ_{m,un}/\Delta S^\circ_{m,un}$, where $\Delta S^\circ_{m,un}$ is the entropy change at $T_m$), and $\Delta C_p$ is the change in heat capacity for the transition (assumed to be temperature independent). We fitted eqs 4−5 and 8−9 to data using the nonlinear least-squares program NONLIN, with $\Delta C_p$ either fixed at zero or floated.

For a three-state unfolding transition, N ⇌ I ⇌ U, where I is an equilibrium folding intermediate, the above set of equations, for either denaturant-induced or thermal-induced unfolding, are simply extended to include two equilibrium constants, $K_{I/N} = [I]/[N]$, and $K_{U/I} = [U]/[I]$, and the corresponding signals for the pure states (i.e., $Y_N$, $Y_I$, and $Y_U$), and the corresponding $\Delta G^\circ_{o,un,i}$ and $m_i$ parameters (or $\Delta H^\circ_{m,un,i}$, $T_{m,i}$, and $\Delta C_{p,i}$ values for thermal unfolding) (Eftink, 1994; Ramsay et al., 1995). In fitting a three-state model, we have assumed linear baseline slopes for the N and U states, and we have assumed that the baseline slope for the I state is the average of the slopes for the N and U state.

We have performed nonlinear least-squares fits of individual data sets (i.e., of $CD_{235\ nm}$ vs $[d]$), but the fits that we show in Figures 4−6 and the parameters given in Table 3 are for a global analysis over three simultaneously obtained data sets for the same sample. In performing these global nonlinear least-squares fits, we have used experimentally determined standard deviation for each data point to weight the analysis. This enables a global analysis to be performed over different types of data and enables us to use the value of the reduced chi squared, $\chi^2$, as an indicator of the goodness of fit (i.e., $\chi^2$ approaching unity is optimum).

## RESULTS

*Absorption, Circular Dichroism, Steady-State Fluorescence Spectra, Solute Quenching, and Optically Detected Magnetic Resonance Data*. Shown in Figure 1A are the absorption spectra of equimolar solutions of WT, V66W′, and V66W nuclease. Upon comparing the spectra of WT and V66W′, which contain only single tryptophans Trp-140 and Trp-66, respectively, we see that the absorbance of the WT protein is slightly red-shifted. To a first approximation, the absorption spectrum of V66W reflects the contribution from both tryptophan residues (there are seven tyrosines and three phenylalanines in each protein). Difference spectra, obtained by subtracting the spectrum of either WT or V66W′ from that of V66W, are also shown in Figure 1B; the V66W-WT difference spectrum should represent the absorption spectrum of Trp-66 in V66W and the V66W−V66W′ difference spectrum should represent that of Trp-140 in V66W. Assuming additivity, these difference spectra show the absorbance of Trp-66 to be slightly bluer than that of Trp-140.

Shown in Figure 1C are fluorescence spectra for WT, V66W′, and V66W nuclease for solutions having the same absorbance at the excitation wavelength of 295 nm. The fluorescence intensities of the three proteins are similar; quantum yields are given in Table 1. The $\lambda_{max}$ of V66W′ is 326 nm, as compared to the $\lambda_{max}$ of 337 nm for WT. The blue-shifted spectrum of Trp-66 in V66W′ is quite remark-

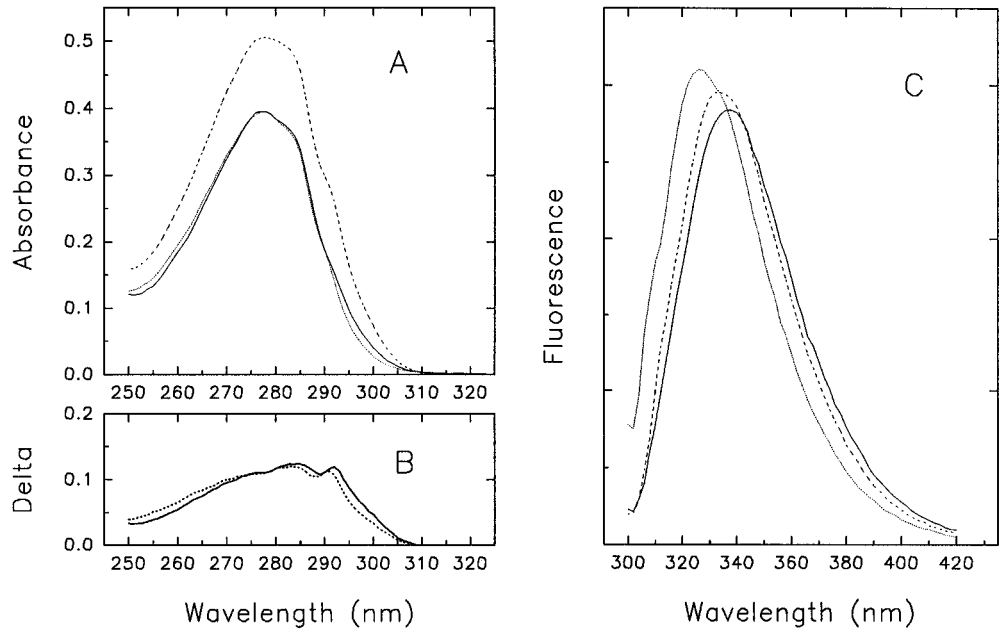


FIGURE 1: (A) Absorbance spectra of WT nuclease (—), V66W (- - -), and V66W′ (•••). Measurement made at room temperature. (B) Difference spectra, defined as the absorbance of V66W minus V66W′ (—) and the absorbance of V66W minus WT (- - -). (C) Fluorescence spectra of WT nuclease (—), V66W (- - -), and V66W′ (•••). Proteins were dissolved in 0.05 M Pipes buffer, pH 7.0. Spectra were taken at 20 °C.

Table 1: Fluorescence Parameters for WT, V66W′, and V66W Nuclease[a]

| | WT | V66W′ | V66W |
|---|---|---|---|
| emission $\lambda_{max}$ (nm) | 337 | 326 | 333 |
| quantum yield | 0.228 | 0.235 | 0.234 |
| quenching rate constants | | | |
| iodide ($\times 10^{-9}$ $M^{-1}$ $s^{-1}$) | 0.21 | 0.21 | 0.19 |
| acrylamide ($\times 10^{-9}$ $M^{-1}$ $s^{-1}$) | 1.0 | 0.68 | 0.60 |
| intensity decay | | | |
| $\tau_1$ (ns) | 5.70 (5.37) | 5.19 (5.08) | 5.45 |
| $\tau_2$ (ns) | 2.49 (0.49) | 1.48 (1.48) | 2.49 |
| $\alpha_1$ | 0.750 (0.810) | 0.605 (0.584) | 0.688 |
| anisotropy decay | | | |
| $\phi_1$ (ns) | 12.8 (12.7) | 16.7 (12.4) | 11.79 |
| $r_o g_1$ | 0.294 (0.297) | 0.240 (0.262) | 0.304 |
| $\phi_2$ (ns) | 0.53 (0.36) | 0.53 (0.009) | 0.83 |
| $r_o g_2$ | 0.054 (0.025) | 0.144 (0.045) | 0.026 |

[a] Conditions: 0.05 M Pipes buffer, pH 7, 20 °C. Emission $\lambda_{max}$ and yields are with excitation at 295 nm. Fluorescence decay and anisotropy parameters are from data with excitation at 300 nm. Values in parentheses are in the presence of 3′,5′-bisphospho-2′-deoxythymidine and $Ca^{2+}$.

able; only the single tryptophans in a few other proteins (e.g., azurin and ribonuclease $T_1$) are known to be bluer (Eftink, 1991). The spectrum of V66W′ also shows a small degree of fine structure, which is characteristic of a tryptophan residue in an apolar environment. The emission maximum of V66W is blue-shifted with respect to WT nuclease and, to a first approximation, is the average of the emission from Trp-40 and Trp-66.

Solute quenching studies using acrylamide and iodide were performed to assess the dynamic exposure of the tryptophan residues (see Figure 2). The apparent rate constant for iodide quenching ($K_{sv}/\langle\tau\rangle = k_{q\,(app)}$, where $K_{sv}$ is from Stern−Volmer plots) was found to be about $0.2 \times 10^9$ $M^{-1}$ $s^{-1}$ for each protein. Using the neutral quencher acrylamide, the Stern−Volmer plots are upward curving, as shown in Figure 2, for each protein. The upward curvature can be attributed to the simultaneous existence of a dynamic and static quenching component (Eftink & Ghiron, 1981). Fitting the acrylamide quenching data with eq 3 yields reasonable $K_{sv}$ and $V$ values for WT and V66W. For V66W′, however, the curvature in the Stern−Volmer plot is very pronounced, and the fit appears to show a very large static component. Since V66W′ is less stable than the WT, it is likely that this dramatically curving plot is due, at least in part, to acrylamide-induced unfolding of this protein fragment. In view of the uncertainty in separating the static and dynamic components, we have taken the sum of $K_{sv}$ and $V$ (which is also equal to the initial slope of a Stern−Volmer plot) as the effective quenching constant, $K_{sv,eff}$. From the ratio, $K_{sv,eff}/\langle\tau\rangle$, we obtain apparent $k_q$ values of 1.0, 0.68, and $0.60 \times 10^9$ $M^{-1}$ $s^{-1}$ for WT nuclease, V66W′, and V66W, respectively (the $k_q$ values were calculated using the mean fluorescence lifetimes measured below).

The iodide and acrylamide $k_q$ values show that Trp-66 of the fragment has a degree of exposure that is less than or equal to that of Trp-140 of the WT protein. In V66W, the acrylamide quenching pattern seems to indicate that the two tryptophan residues have less exposure in this mutant than is the case for the individual tryptophan residues in the WT and V66W′.

Near- (aromatic) and far-UV CD spectra for V66W′, V66W, and WT nuclease are shown in Figure 3. The far-

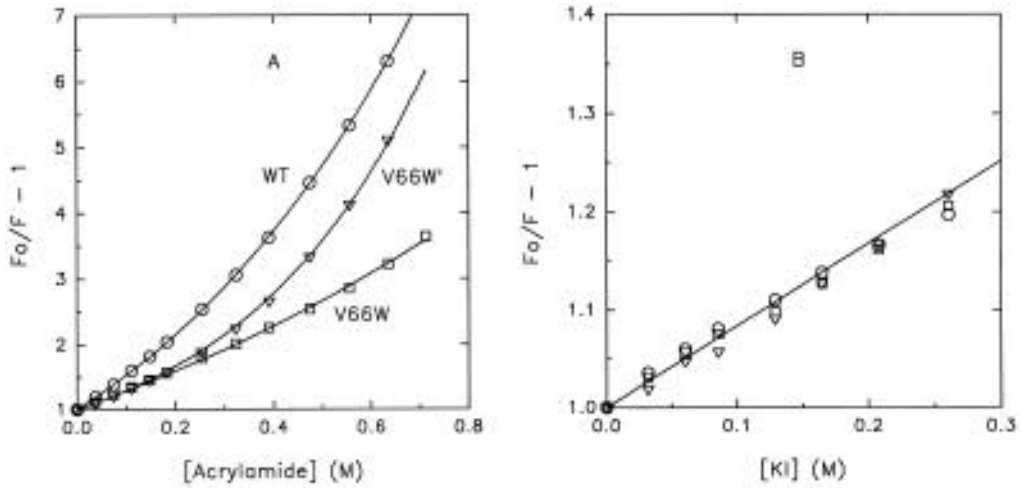


FIGURE 2: (A) Acrylamide solute quenching of WT nuclease (○), V66W′ (▽), and V66W (□). Conditions: 0.05 M Pipes, pH 7.0, 20 °C. Solid lines are fits of eq 3 with the following parameters: $K_{sv} = 3.92$ M$^{-1}$ and $V = 0.93$ M$^{-1}$ for WT; $K_{sv} = 0.05$ M$^{-1}$ and $V = 2.5$ M$^{-1}$ for V66W′; and $K_{sv} = 2.31$ M$^{-1}$ and $V = 0.43$ M$^{-1}$ for V66W. (B) Iodide quenching of WT nuclease (○), V66W′ (▽), and V66W (□). The solid line is a fit eq 3 to the WT data with $K_{sv} = 0.84$ M$^{-1}$. Not shown (for clarity) are fits of $K_{sv} = 0.93$ M$^{-1}$ for V66W′ and $K_{sv} = 0.85$ M$^{-1}$ for V66W.

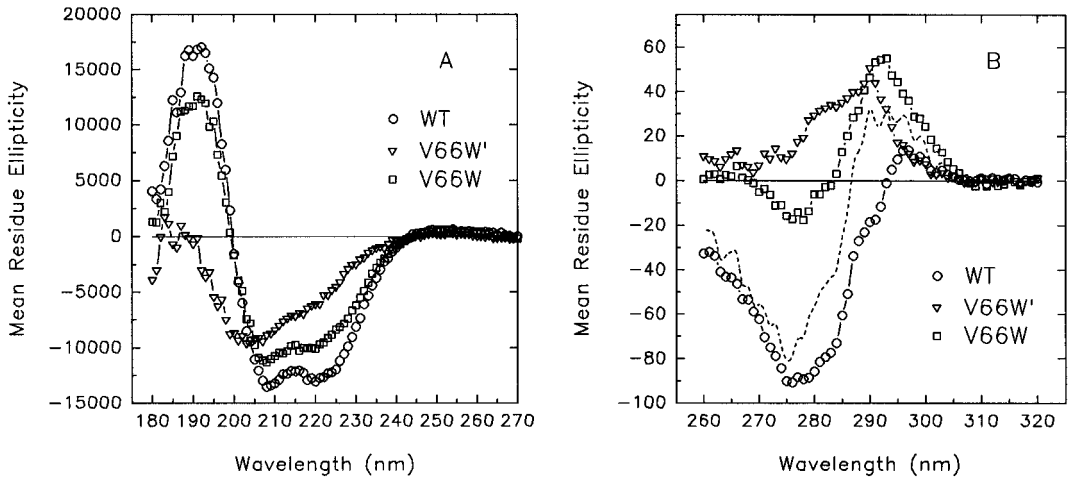


FIGURE 3: Circular dichroism spectra (far-UV, left panel; near-UV, right panel) of WT nuclease (○), V66W′ (▽), and V66W (□). Proteins were dissolved in 0.05 M Pipes buffer, pH 7.0. Mean residue ellipticities have units of deg·cm$^2$/dmol. Spectra were recorded at 20 °C. Also shown for the near-UV range is the sum of the spectra of WT and V66W′ (- - -).

UV CD spectra, down to 180 nm, show that the magnitude of the ellipticity decreases in the order of WT > V66W > V66W′. Analysis using the algorithm of Sreerama and Woody (1993) yields the following estimates of secondary structure: for WT, 0.340 α-helix, 0.310 $\beta$-sheet, 0.223 turns, and 0.145 other; for V66W, 0.325 α-helix, 0.296 $\beta$-sheet, 0.219 turns, and 0.149 other; for V66W′, 0.117 α-helix, 0.412 $\beta$-sheet, 0.256 turns, and 0.191 other. The V66W′ fragment is found to have about one-thid the α-helix content and more $\beta$-sheet content, as compared to the full length protein. Flanagan et al. (1992) have published a similar far-UV CD spectrum for a non-tryptophan-containing Δ137−149 nuclease fragment. The aromatic CD spectrum of WT nuclease shows a negative mean residue ellipticity peak of −90 deg·cm$^2$/dmol at 276 nm. V66W′ shows a positive ellipticity peak of +50 deg·cm$^2$/dmol at 290 nm. The aromatic CD spectrum of V66W shows contributions from both Trp-140 and Trp-66. However, the positive ellipticity peak for V66W at 292 nm is larger than expected from a contribution from Trp-66. Also, the negative ellipticity peak for V66W at 276 nm is smaller than expected from a contribution from Trp-140, suggesting that there are slight differences in the microenvironment of the tryptophans in V66W, as compared to the fragment and WT.

Slow passage ODMR spectra for the three proteins are shown in Figure 4. Each spectrum was obtained by monitoring the phosphorescence 0,0-band peak; their wavelengths differed by less than 0.5 nm, although the 0,0-band width of V66W was slightly larger than that of the wild-type nuclease (phosphorescence spectra not shown). The spectrum of V66W (Figure 4B) has been fitted to two pairs of Gaussian-shaped bands, while those of wild-type nuclease (Figure 4A) and V66W′ (Figure 4C) have been fitted to one pair of Gaussian-shaped bands. The fit is extremely good for the wild-type nuclease, but fast passage effects are apparent in the other spectra, although measured using the same sweep rate. These effects account for deviations from the Gaussian line shapes on the high frequency edges of the transitions. The ODMR peak frequencies, bandwidths, and the zero field splitting D and E parameters are listed in Table 2, along with the 0,0-band peak wavelengths and the lifetimes of the major decay component. A plot of the ODMR peak frequencies of the D-E and 2E transitions vs wavelength,

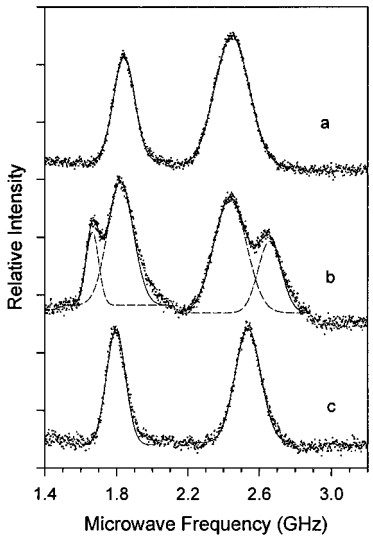


FIGURE 4: Phosphorescence-detected slow-passage ODMR signals of tryptophan in (a) WT, (b) V66W, and (c) V66W′. The phosphorescence is monitored at the respective 0,0-band peaks given in Table 2 using 3 nm band-pass and an experimental temperature of 1.2 K. The microwave frequency was swept at 40 MHz/s, and signal averaging was carried out to improve the signal/noise. The solid lines are fittings of one pair (a and c) or two pairs (b) of Gaussian-shaped bands, while the dashed lines are a deconvolution of two bands of Trp-140 and Trp-66.

Table 2: Triplet State Properties for WT, V66W′, and V66W Nuclease

| | WT | V66W′ | V66W |
|---|---|---|---|
| phosphorescence parameters[a] | | | |
| $\lambda_{0,0}$ (nm) | 407.2 | 407.4 | 407.6 |
| $\tau$ (s) | 7.2 (74%)[b] | 6.6 (90%) | 7.3 (79%) |
| ODMR data[c] | | | |
| D-E (GHz) | 1.805 | 1.765 | 1.803, 1.650 |
| fwhm (MHz) | 133 | 116 | 126, 91 |
| 2E (GHz) | 2.409 | 2.501 | 2.391, 2.636 |
| fwhm (MHz) | 241 | 169 | 213, 153 |

[a] Data at 77 K. [b] Major lifetime component in deconvolution of phosphorescence decay. [c] All ODMR data are for measurements at 1.2 K. ODMR frequencies (estimated error ± 10 MHz) were obtained using slow passage and were corrected for fast passage effects by extrapolation to zero sweep rate. Line widths (fwhm) were obtained at a 30 MHz/s microwave sweep rate.

monitored through the 0,0-bands of the three protein samples, is given in Figure 5.

ANS binding (fluorescence enhancement) studies were performed on the three proteins, since this method has frequently been used to characterize the amount of apolar surface area in proteins. As a reference, we compared the degree of enhancement of ANS fluorescence for the proteins at pH 7 (0.05 Pipes, 20 °C) to the enhancement of ANS fluorescence for the same proteins at pH 2.2, 1.0 M KCl (conditions believed to convert the protein into the "A" state; Fink et al., 1993). We found the enhancements to be 30%, 45%, and 18% for WT nuclease, V66W′, and V66W, respectively. That is, ANS binding senses additional apolar surface area in the V66W′ fragment, but the degree of enhancement is not large in comparison with that found for ANS binding to the low pH "A" state of nuclease (Fink et al., 1993). Note that the above enhancements depend on the degree of ANS binding to the native state and to the state of the respective proteins at pH 2.2, 1.0 M KCl, thus

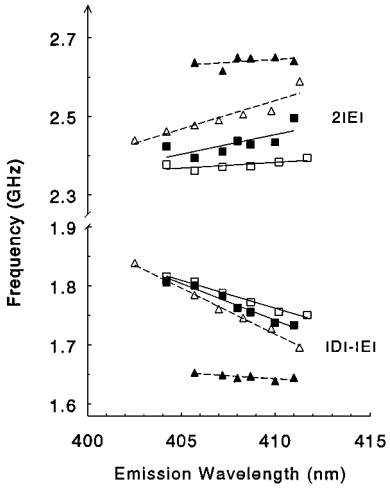


FIGURE 5: Comparison of the wavelength dependence of the |D| − |E| and 2|E| triplet state ODMR frequencies as a function of emission wavelength within the 0,0-band of tryptophan in WT nuclease (open squares, Trp-140), V66W′ (open triangles, Trp-66), and V66W (filled triangles for Trp-66 and filled squares for Trp-140). All data have been corrected for rapid-passage effects. The emission bandwidth was ca. 1 nm, and the temperature was 1.2 K.

making it difficult to interpret the slight differences between the enhancements for WT and V66W.

*Thermal and Guanidine-Induced Unfolding Studies*. The guanidine-induced unfolding of WT type nuclease, V66W′, and V66W are shown in Figure 6. Changes in the CD signals at 222 and 235 nm (228 and 235 nm in the case of V66W′) as well as changes in fluorescence (excitation at 295 nm, emission at 340 nm) were simultaneously monitored on the same sample using our multidimensional spectrophotometer (Ramsay & Eftink, 1994a,b; Ramsay et al., 1995). These three data sets were subjected to a global analysis to fit a two-state model to the data. The solid lines in panels A−C show this fit to the two-state model; an excellent fit is obtained for WT and V66W′, but the fit for V66W is not as good (compare the $\chi^2$ of 2.0, 0.69, and 11.6 for two-state fits for the three proteins in Table 3). Figure 7 shows the residual pattern (experimental signal minus calculated signal, filled circles) for the two-state fits for V66W. The nonrandom residual pattern is obvious for this protein. (Residual plots for WT and V66W′ are not shown; they are random, as is indicated by the relatively low $\chi^2$.)

The data for V66W were then fitted with a three-state model, shown as the dashed lines through the raw data in Figure 6C and by the open circles in the residual patterns in Figure 7. The three-state model provides an excellent fit for V66W, as indicated by the reduction of $\chi^2$ from 11.58 (two-state) to 1.26 (three-state).

Shown in Table 3 are thermodynamic parameters for the guanidine-induced unfolding of these proteins. The two-state $\Delta G°_{o,un}$ and $m$ values for wild-type nuclease are 5.32 kcal/mol and 5.83 kcal/(mole·M), values that are reasonably consistent with previously determined values (Shortle & Meeker, 1986; Shortle et al., 1990; Hynes et al., 1989; Eftink et al., 1991a; Gittis et al., 1993; values listed in legend of Table 3). The V66W′ fragment unfolds in a two-state manner with $\Delta G°_{o,un}$ and $m$ values that are both less than half the values for WT. The three-state fit for V66W yields stepwise free energy changes and m values. The recovered values of $\Delta G°_{o,I/N}$ and $\Delta G°_{o,U/I}$ and the corresponding $m$ values are given in Table 3; these values depend on whether

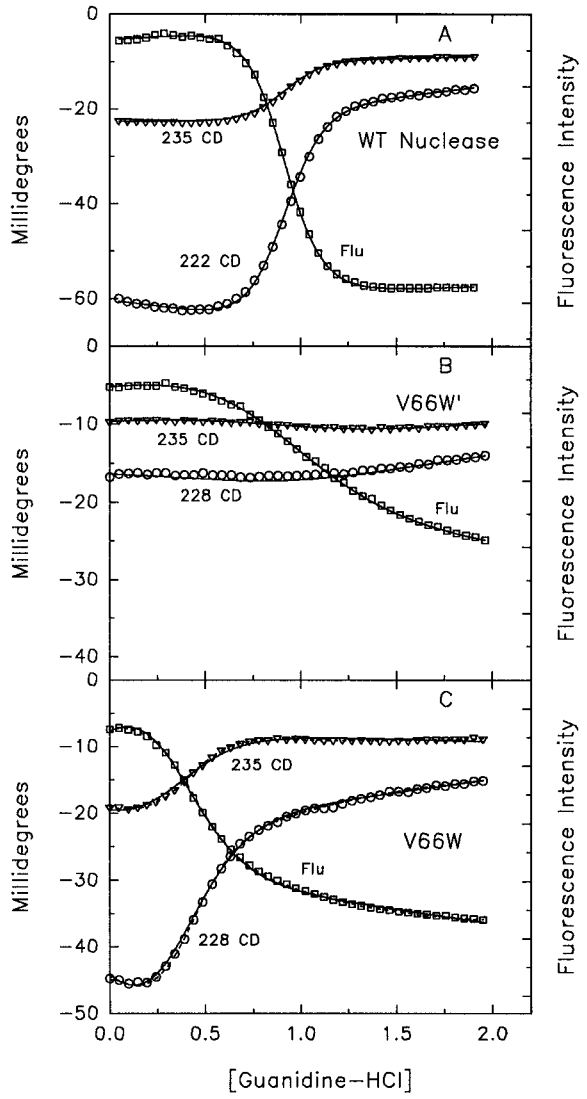


FIGURE 6: Simultaneously obtained changes in CD and fluorescence signals for the guanidine-HCl induced unfolding of WT nuclease (A), V66W′ (B), and V66W (C) at 20 °C. The solid lines are fits of the two-state model (eqs 4−7) with the $\Delta G°_{un}$ and $m_{un}$ in Table 3. The dashed lines through the experimental points for V66W (panel C) are the fit with a three-state unfolding model as described in the text and Table 3.

all of the parameters are floated in the fit or whether some of the parameters are restricted according to a model to be described in the Discussion.

The temperature-induced unfolding of the three proteins was also studied using our multidimensional CD/fluorescence instrument. As shown in Figure 8, both WT and V66W′ were well described by a two-state unfolding model, with $T_m$, $\Delta H°_{m,un}$, and $\Delta C_p$ values given in Table 3. Parameters are given both for analyses in which $\Delta C_p$ is allowed to float and in which $\Delta C_p$ is fixed at zero. By comparing the reduced $\chi^2$ values, it is seen that a very slight improvement in the fit is achieved by floating the $\Delta C_p$ (as expected for WT, since its $T_m$ is not low enough to easily enable recovery of a $\Delta C_p$ value from data of the type in Figure 8). For the V66W′ fragment the $T_m$ is only a few degrees below the value for WT, but the $\Delta H°_{m,un}$ (and $\Delta C_p$) are much smaller than the value for WT.

The thermal transition for V66W, on the other hand, is not fit as well by a two-state model, as compared to the fits

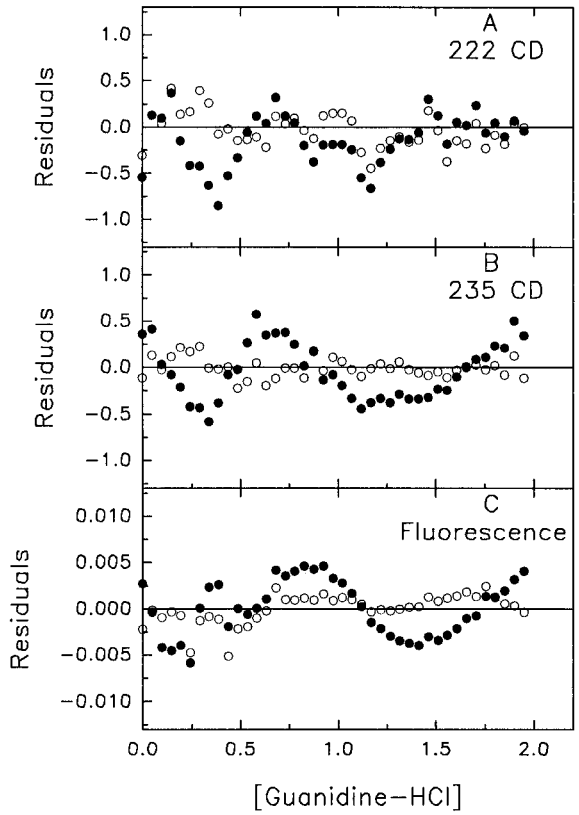


FIGURE 7: Residual patterns for the two-state global fit (filled circles) and the three-state global fit (open circles) of the three data sets for V66W.

for the other two proteins. This is again seen by the values of $\chi^2$ of 5.28 for V66W, compared to values closer to unity for WT and V66W′. A three-state model (compare $\chi^2$ in Table 3 and see Discussion) was found to provide a much better fit for this protein. The resulting thermodynamic parameters are given in Table 3, both for fits in which all parameters were floated and for fits in which some parameters were restricted, as presented in the Discussion.

*Time-Resolved Fluorescence Intensity and Anisotropy Decay Data*. Fluorescence lifetime and anisotropy decay data for wild-type nuclease A has been reported previously by our lab and by others (Brochon et al., 1974; Grinvald & Steinberg, 1976; Eftink et al., 1991b; Royer et al., 1993). The biexponential fluorescence decay of the wild-type protein is dominated by a 5−6 ns component at room temperature. The anisotropy decay is dominated by a 12−13 ns rotational correlation time, which is attributed to global rotation of the protein; a subnanosecond rotational correlation time, which contributes less than 15% to the initial anisotropy, indicates a small degree of segmental rotation of Trp-140.

Phase modulation lifetime data (not shown) were collected for the three proteins; fits to a biexponential decay law are given in Table 1. For WT nuclease, the values of $\tau_1 = 5.70$ ns, with a minor component having $\tau_2 = 2.49$ ns, are consistent with literature values. Differential polarized phase modulation (anisotropy decay) data for WT and V66W′ are shown in Figure 9. These data were described by a biexponential decay law. For WT the fit yields a long rotational correlation time, $\phi_1$, of 12.8 ns and a short rotational correlation time, $\phi_2$, of 0.53 ns. For the V66W′ fragment, fluorescence lifetime values of $\tau_1 = 5.19$ and $\tau_2 = 1.48$ ns are found. Anisotropy decay data are described

Table 3: Thermodynamic Parameters for the Unfolding of WT, V66W′, and V66W Nuclease[a]

| | Guanidine-HCl Induced Unfolding | | | | |
|---|---|---|---|---|---|
| | $\Delta G°_{o,un1}$ | $m_1$ | $\Delta G°_{o,un2}$ | $m_2$ | $\chi^2$ |
| WT | 5.32[b] (5.16−5.47) | 5.83[b] (5.67−5.99) | | | 2.03 |
| V66W′ | 1.87 (1.69−2.05) | 2.12 (1.91−2.30) | | | 0.69 |
| V66W | 1.30 (1.07−1.53) | 3.87 (3.63−4.11) | | | 11.58 |
| | 2.13 (2.01−2.32) | 4.51 (4.02−5.00) | 0.51 (0.30−0.79) | 1.07 (1.11−1.53) | 1.26 |
| | 1.89 (1.71−2.07) | 4.39 (4.08−4.71) | ⟨1.87⟩ | ⟨2.12⟩ | 1.47 |

| | Thermal Unfolding | | | | | | |
|---|---|---|---|---|---|---|---|
| | $\Delta H°_{un,1}$ | $T_{m,1}$ | $\Delta C_{p,1}$ | $\Delta H°_{un,2}$ | $T_{m,2}$ | $\Delta C_{p,2}$ | $\chi^2$ |
| WT | 78.7 (75.7−81.7) | 53.1 (53.0−53.3) | ⟨0⟩ | | | | 1.24 |
| | 79.6 (76.7−82.1) | 53.1 (53.0−53.3) | 2.55 (2.32−2.76) | | | | 0.86 |
| V66W′ | 29.3 (27.0−30.3) | 49.7 (48.8−50.6) | ⟨0⟩ | | | | 0.83 |
| | 28.1 (25.8−30.3) | 47.5 (46.7−48.2) | 0.81 (0.61−0.98) | | | | 0.77 |
| V66W | 42.8 (39.5−46.2) | 43.1 (42.6−43.6) | ⟨0⟩ | | | | 5.66 |
| | 43.4 (40.6−45.9) | 43.8 (43.2−44.3) | −1.49 (−1.78 to −1.16) | | | | 5.28 |
| | 41.8 (39.7−43.6) | 44.4 (44.1−44.8) | ⟨0⟩ | 22.3 (19.2−25.7) | 50.3 (47.7−52.8) | ⟨0⟩ | 1.29 |
| | 46.6 (43.3−49.6) | 44.7 (43.5−45.5) | 1.58 (1.30−1.86) | 18.4 (12.8−25.5) | 44.8 (40.8−49.7) | 0.83 (0.54−1.11) | 1.03 |
| | 45.8 | 43.5 | 1.69 | ⟨28.1⟩ | ⟨47.5⟩ | ⟨0.81⟩ | 1.11 |

[a] Parameters from a global fit of equation 4-8 to CD data at 222 and 235 nm, plus fluorescence data (see Figure 6). Values in brackets ⟨⟩ were not allowed to float. $\Delta G°$ and $\Delta H°$ values are in kcal/mol; $\Delta C_p$ values are in kcal/(mol·K); $m$ values are in kcal/(mol·M); $T_m$ values are in °C. Conditions: 0.05 M Pipes buffer, pH 7, 20 °C (for the guanidine-induced unfolding). [b]Compare to values of $\Delta G°_{o,un}$ and $m$ values of 5.6 and 5.07 from Shortle and Meeker (1986), 6.85 and 5.48 from Shortle et al. (1990), 4.6 and 5.9 from Hynes et al. (1989), 5.50 and 5.67 from Eftink et al. (1991a), and 5.2 and 6.4 from Gittis et al. (1993).

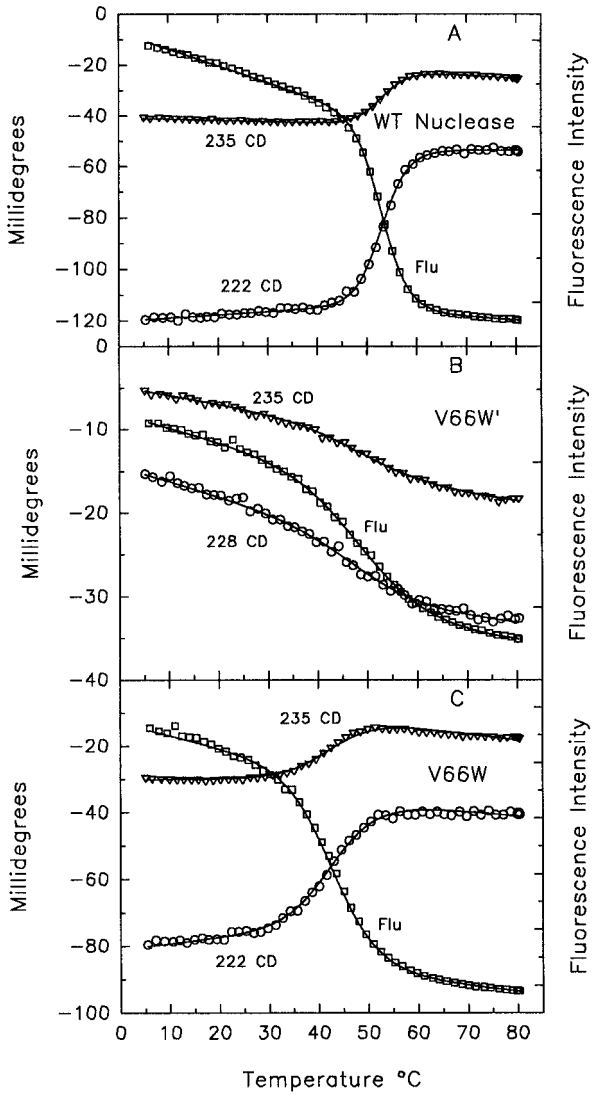


FIGURE 8: Simultaneously obtained changes in CD and fluorescence data for the thermally induced unfolding of WT nuclease (A), V66W′ (B), and V66W (C). The solid lines are fits of the two-state model with $\Delta H°_{un}$ and $T_m$ values given in Table 3.

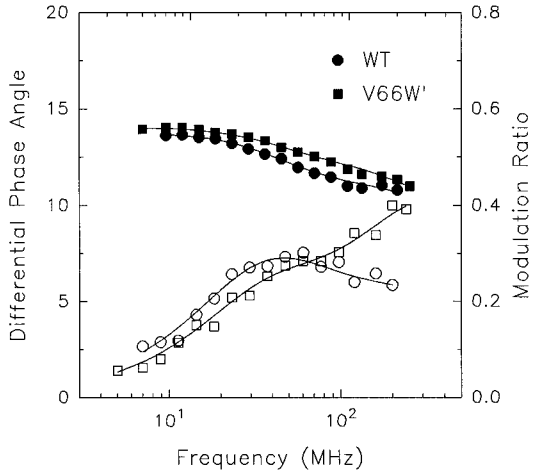


FIGURE 9: Differential phase and modulation data for WT (○, ●) and V66W′ (□, ■). Hollow symbols are phase data and filled symbols are modulation data; circles are data for WT nuclease; squares are data for V66W′. The fits are a biexponential decay law with the rotational correlation times given in Table 1.

by $\phi_1 = 16.7$ and $\phi_2 = 0.53$ ns. The shorter rotational correlation time contributes 37% to the initial anisotropy, which is much larger than the corresponding contribution of the sub-nanosecond $\phi$ for WT. Fluorescence lifetime data for the two tryptophans in V66W were also described as a biexponential with $\tau_1 = 5.45$ ns and $\tau_2 = 2.49$ ns. The anisotropy decay data for V66W were described by a dominant $\phi_1$ value of ∼12 ns, which is similar to that for WT.

Also listed in Table 1 are fluorescence lifetimes and anisotropy decay parameters for WT and V66W′ nuclease in the presence of the specific ligand 3′,5′-bisphospho-2′-deoxythymidine (plus $Ca^{2+}$). There is a slight decrease in the fluorescence decay time of Trp-140 of WT nuclease and essentially no change in the decay time of Trp-66 in V66W′ upon binding of ligand. Anisotropy decay data show no change in the longer rotational correlation time, $\phi_1$, of WT upon binding of ligand. However, the $\phi_1$ for V66W′ shows

a significant decrease from ~17 to ~12 ns upon ligand binding.

## DISCUSSION

The Δ137−149 fragments of nuclease have been studied as a possible model for a folding intermediate (Flanagan et al., 1992, 1993). The results presented here, which exploit the spectral properties of Trp-66 in the V66W′ fragment, provide further insights to the solution structure and dynamics of this molecule.

*CD Results*. The aromatic CD spectrum of V66W′ (see Figure 2B) shows a relatively strong signal at 290, which (at this wavelength) can only be attributed to the asymmetric environment experienced by Trp-66. This signal indicates a persistent three-dimensional structure around Trp-66 for this fragment. By comparison, the aromatic CD of denatured proteins (including V66W′ in 2 M guanidine-HCl; data not shown) and molten globule states generally show no amplitude in the aromatic CD region, due to the lack of a persistent chiral environment for the aromatic chromophores (Kuwajima, 1989, 1995).

*Fluorescence Results*. The relatively large fluorescence quantum yield, the blue $\lambda_{max}$ of 326 nm, the relatively small quenching rate constant, and the structured emission indicate that Trp-66 in V66W′ is in an apolar environment and is protected from interaction with solvent and quenching side chains. Because a tryptophan residue is unnatural for position 66, it is remarkable that a Trp-66 appears to experience an apolar, buried environment such as that experienced by Trp-59 in ribonuclease $T_1$. The anisotropy decay data for V66W′ are quite different from that of WT or V66W nuclease. The latter proteins have a long $\phi_1$ of 12 ns, which is approximately the value expected for global rotation of a hydrated spherical protein of molecular mass 16.8 kDa [as calculated with the equation $\phi_{sphere} = M(\upsilon + h)/kT$, where $M$ is the molecular mass, $\upsilon$ is the partial specific volume, 0.73 mL/g, of the protein, $h$ is the degree of hydration, taken to be 0.3 mL/g], and show only a small amplitude associated with subnanosecond segmental motion of the tryptophan residues. The V66W′ fragment, on the other hand, has a longer $\phi_1$ value of 17 ns and shows a much larger amplitude for subnanosecond segmental motion of Trp-66. The larger $\phi_1$ can be interpreted as indicating that this fragment has an expanded structure. Flanagan et al. (1992, 1993) have previously reached a similar conclusion for a non-tryptophan-containing Δ137−149 fragment using small angle X-ray scattering. The large $r_o g_2$ value for the short $\phi_2$ can be interpreted in terms of rapid, hindered rotation of Trp-66 within a cone of semi-angle 31° (Lipari & Szabo, 1980). When the specific ligand, pdTp (plus $Ca^{2+}$), binds to V66W′, the values of $\phi_1$ and $\phi_2$ (and the amplitude of the latter) approach the values found for WT nuclease. This is consistent with the stabilization of a more structured state of V66W′ upon ligand binding. The anisotropy decay data monitor the changes in the environment of Trp-66. From CD, $^1$NMR, and SAXS studies, Flanagan et al. (1992) have shown that global changes occur in the WT Δ137−149 fragment upon pdTp binding.

*Triplet State Studies*. The ODMR studies provide additional insight into the local tryptophan environments of these proteins. Figure 4 shows that the zero field splitting parameters, D and E, of Trp-66 are severely perturbed when V66W is converted to the V66W′ fragment. Smaller changes in the zero field splitting of Trp-140 occur when WT nuclease is converted to V66W. These changes may be studied quantitatively as a function of triplet state energy by examining Figure 5, which shows that the D-E ODMR frequency of Trp-140 in both WT and V66W depends rather strongly on wavelength, in a manner typical for a tryptophan residue that is partially exposed to solvent (Kwiram, 1982). Randomly oriented polar solvent molecules also provide an inhomogeneous distribution of local environments that contribute to a relatively large ODMR line width. As listed in Table 2, the ODMR line widths of Trp-140 in both WT and V66W are considerably larger than those of Trp-66 in V66W, indicating that Trp-140 is in a more heterogeneous environment.

The 0,0-band wavelength of tryptophan phosphorescence also has been shown to depend on the polarity of the local environment (Galley & Purkey, 1970). Blue-shifted phosphorescence (in a rigid solvent) generally is associated with a polar environment in which the solvent molecules are oriented to stabilize the ground state electron distribution. Red-shifted emission (i.e., 0,0-band wavelength generally greater than 410 nm) is found in a nonpolar but polarizable local environment, which stabilizes the larger dipole moment of the excited triplet state. The relatively blue-shifted 0,0-band of Trp-140 thus classifies it as a residue that is exposed to a polar environment. Trp-66 of V66W′ is more anomalous. One would perhaps expect Trp-66 to be located in a buried, polarizable environment, based on the above fluorescence studies with V66W′. Such an environment is characterized by relatively narrow ODMR bands and a very slight wavelength dependence of their ODMR frequencies (Kwiram, 1982; Maki, 1984). On the basis of these latter criteria, Trp-66 appears to be a buried residue. Similar anomalous ODMR data (a narrow ODMR line width, whose frequencies are relatively independent of wavelength, yet having a blue-shifted 0,0-band) have been previously observed for Trp-59 of ribonuclease $T_1$. The crystal structure of the latter protein shows Trp-59 to be buried but to also form a hydrogen bond with an interior water molecule. It has been suggested (Hershberger et al., 1980; Lam et al., 1992) that the blue-shift of the phosphorescence 0,0-band results from this polar interaction. We suggest that Trp-66 of V66W may be in a similar homogeneous buried environment, but that it is also subjected to specific polar interactions that tend to stabilize the ground state relative to the excited triplet state.

*Evidence for Differences in Trp-66 between V66W and V66W′*. The environment of Trp-66 in the V66W′ fragment is clearly modified from that in V66W. This is most apparent from the ODMR frequencies in Figure 5. The wavelength dependence of the D-E frequency is now large and resembles that of Trp-140. In addition, both the D-E and 2E ODMR frequencies have approached those of Trp-140. The ODMR line widths of Trp-66 in V66W′ have increased relative to those found in V66W but are still smaller than those of Trp-140. These changes are consistent with an increase in the heterogeneity of the local environment of Trp-66 on forming the 1−136 fragment. As judged by the ODMR line widths, however, there remains a degree of local structural integrity that exceeds that of a totally solvent-exposed residue or even that of the partially exposed Trp-140.

This conclusion, that the environment of Trp-66 has subtle differences between V66W′ and V66W, can also be concluded from the aromatic CD spectral data. The fact that the aromatic CD spectrum of V66W does not appear to be the sum of that for WT and V66W′ (dashed line in Figure 3) suggests that either tryptophan residue has a slightly different environment in V66W.

*Interpretation of Thermodynamic Results*. The observation of two-state unfolding of WT nuclease, with both guanidine-HCl and thermally induced unfolding at neutral pH and moderate ionic strength, is consistent with several previous studies (Shortle & Meeker, 1986; Shortle et al., 1988; Griko et al., 1988; Gittis et al., 1993; Carra et al., 1994). The excellent global fitting of simultaneously obtained CD and fluorescence data is a test of the two-state model (Lumry et al., 1966). Our recovered $\Delta G°_{o,un} = 5.3$ kcal/mol and $m = 5.8$ kcal/(mol·M) for guanidine-HCl induced unfolding and our $\Delta H°_{un} = 80$ kcal/mol, $T_m = 53$ °C, and $\Delta C_p = 2.5$ kcal/(mol·°C) for thermal unfolding are in good agreement with previous reports (including $\Delta H_{cal}$ and $\Delta C_p$ from DSC data), considering slight differences in buffer conditions (Griko et al., 1988; Shortle et al., 1988; Tanaka et al., 1993; Carra et al., 1994). The calorimetrically determined $\Delta C_p$ for WT nuclease is somewhat lower [2.15 kcal/(mol·°C), Carra et al., 1994; 2.21 kcal/(mol·°C), Tanaka et al., 1993] than our value, which is based on a van't Hoff analysis of the data in Figure 7. Admittedly, our $\Delta C_p$ has a fairly large confidence range, due to the fact that the $\Delta C_p/\Delta H°_{o,un}$ is small for WT, and, consequently, the shape of the thermal transition is nearly symmetrical. Still, our fitted $\Delta C_p$ is reasonably close to the DSC $\Delta C_p$ value.

We also find that the guanidine-HCl and thermally induced unfolding transitions for V66W′ can be described by a two-state model. The data in Figures 6B and 8B show that the presence of an unfolding transition would be very difficult to determine with CD data alone. The change in the fluorescence signal with denaturant and temperature (and the global fits with the CD data) reveals the transition, no doubt due to the presence of Trp-66 as a reporter group. The $\Delta G°_{o,un}$ and $m$ for guanidine-HCl unfolding of V66W′ are both less than one-half the values for the WT protein. Likewise, the $\Delta H°_{un}$ for thermal unfolding of V66W′ is less than one-half the value for WT, yet the transition temperature for V66W′ is nearly the same as that for the WT and the transition still appears to be a cooperative two-state process. The reduced stability of Δ137−149 fragments, which has previously been characterized both qualitatively and quantitatively (Shortle & Meeker, 1989; Flanagan et al., 1992; Shortle & Abeygunawardana, 1993; Gittis et al., 1993), is remarkable since the deletion of the last 13 C-terminal residues must cause a large destabilization of the native state. From the above CD studies with V66W′ and NMR studies with a related G88V fragment, it is believed that the five-stranded $\beta$-barrel structure at the N-terminal two-thirds of the protein is retained in the fragments (Shortle & Abeygunawardana, 1993). Actually, the Δ137−149 fragment of WT nuclease appears to be much less structured in solution; fragments of certain mutants, such as that formed from V66W and G88V, have more stable folded structures (Shortle & Meeker, 1989; Flanagan et al., 1993). (In unpublished work, we have also found V66W′ to undergo a two-state pressure-induced unfolding transition and to be unfolded by acid.)

Both the guanidine-HCl and thermal induced unfolding of V66W are better described as a three-state process, as previously found by Stites et al. (1993) and Carra et al. (1994). The thermodynamic parameters for the two transitions, N ⇌ I and I ⇌ U, are difficult to determine with confidence due to correlations in the fitting parameters. As a model for fitting and interpreting the data for V66W, we have considered the following two subdomain depiction of the protein (Shortle & Meeker, 1989; Carra et al., 1994; Xie et al., 1994) and have performed a linked analysis. In this model, the second I ⇌ U transition in V66W is assumed to have the same thermodynamic parameters as that for the unfolding of V66W′. Thus, the I ⇌ U transition is assumed to be the unfolding of the $\beta$-barrel region of the protein, and the N ⇌ I transition is assumed to involve the melting away of the C-terminal helix (and possibly the other helical regions) from the rest of the protein. Fixing these parameters in the analysis provides very good fits (see Table 3) for both the denaturant and thermal unfolding of V66W.

This model yields values of $\Delta G°_{o,un1} = 1.89$ kcal/mol and $m_1 = 4.39$ kcal/(mol·M) for the N ⇌ I step, compared to $\Delta G°_{o,un2} = 1.87$ kcal/mol and $m_2 = 2.12$ kcal/(mol·M) for the I ⇌ U step. The sum of the two $\Delta G°_{un}$ is reasonably close to that for the two-state unfolding of WT protein. These values of $\Delta G°_i$ and $m_i$ would produce a maximum mole fraction of the I state of ∼60% at 0.65 M guanidine-HCl. The observation that $m_1$ is relatively large, compared to $m_2$, suggests that the unfolding of the α-helical regions exposes a large amount of hydrophobic surface (Myers et al., 1995). Likewise, with this model the fitted $\Delta H°_{un,1} = 45.8$ kcal/mol and $\Delta H°_{un,2} = 28.1$ kcal/mol, and the sum of these values is approximately equal to the $\Delta H°_{un}$ for the two-state unfolding of WT protein. Values of $\Delta C_p$ for the two unfolding transitions of V66W can also be obtained with this model. These values have a broad confidence range, but they appear to show a larger $\Delta C_{p,1}$ value for the N ⇌ I transition, consistent with the above interpretation that this step exposes the larger amount of apolar surface area.

Why does substitution of valine by tryptophan at position 66 result in non-two-state behavior? As discussed by Carra and Privalov (1995), it is probably best to consider the unfolding of WT nuclease and its mutants to be a N ⇌ I ⇌ U process, with the relative free energy level of the I state determining the degree to which the unfolding process appears to be two-state or not. For WT nuclease, the free energy level of I appears to be near to that of U, so that unfolding is essentially two-state at neutral pH and low ionic strength. For certain mutants, including V66W and the triple mutant V66L+G88V+G79S (Carra & Privalov, 1995), the I state has a relatively lower free energy level and is populated to a greater extent. We know from the fluorescence and aromatic CD studies presented here that Trp-66 in the V66W′ fragment has a nonpolar and anisotropic microenvironment. The microenvironment of Trp-66 is similar, but not exactly the same, in the full length V66W protein; this conclusion is best derived from the ODMR results. This slight difference in Trp-66 between V66W′ and V66W indicates that our above thermodynamic analysis (in which $\Delta G°_{o,un2}$ and $m_2$, etc., for V66W were assumed to be the same as the corresponding values for the unfolding of V66W′) may be an oversimplification. Nevertheless, the thermodynamic parameters for the constrained two subdomain model for V66W indicate that the N ⇌ I transition

has a lower $\Delta G°$ than would be the case for WT nuclease. If the N $\rightleftharpoons$ I transition involves primarily the unfolding of the C-terminal α-helix (the third and longest helix in the protein), then it is interesting to note that position 66 (at the end of the first helix, which is between the third and fourth $\beta$ strands) is not close to the interface between the subdomains. It appears that the need to accommodate and bury the indole ring of Trp-66 causes a rearrangement of the $\beta$ subdomain such that the interactions with the C-terminal α-helix are weakened.

## ACKNOWLEDGMENT

We thank Dr. Wesley Stites, University of Arkansas, for providing us with the plasmids containing the expression system for V66W and V66W′.

## REFERENCES

Alexandrescu, A. T., Hinck, A. P., & Markley, J. L. (1990) *Biochemistry 29*, 4516−4525.
Anfinsen, C. B., Cautrecacaus, P., & Taniuchi, H. (1971) *Enzymes (3rd ed.) 4*, 177−204.
Arni, R., Heinemann, U., Tokuoka, R., & Saenger, W. (1988) *J. Biol. Chem. 263*, 15358−15368.
Brochon, J. C., Wahl, P., & Auchet, J. C. (1974) *Eur. J. Biochem. 41*, 577−583.
Calderon, R. O., Stolowich, N. J., Gerlt, J. A., & Sturtevant, J. M. (1985) *Biochemistry 24*, 6044−6049.
Carra, J. H., Anderson, E. A., & Privalov, P. L. (1994a) *Biochemistry 33*, 10842−10850.
Carra, J. H., Anderson, E. A., & Privalov, P. L. (1994b) *Protein Sci. 3*, 944−951.
Dill, K. A., & Shortle, D. (1991) *Annu. Rev. Biochem. 60*, 795−825.
Eftink, M. R. (1991) *Methods Biochem. Anal. 35*, 127−205.
Eftink, M. R. (1994) *Biophys. J. 66*, 482−501.
Eftink, M. R., & Ghiron, C. A. (1981) *Anal. Biochem. 114*, 199−227.
Eftink, M. R., Ghiron, C. A., Kautz, R. A., & Fox, R. O. (1991a) *Biochemistry 30*, 1193−1199.
Eftink, M. R., Gryczynski, I., Wiczk, W., Laczko, G., & Lakowicz, J. R. (1991b) *Biochemistry 30*, 8945−8953.
Evans, P. A., Kautz, R. A., Fox, R. O., & Dobson, C. M. (1989) *Biochemistry 28*, 362−370.
Fink, A. L., Calciano, L. J., Goto, Y., Nishimura, M., & Swedberg, S. A. (1993) *Protein Sci. 2*, 1155−1160.
Flanagan, J. M., Kataoka, M., Shortle, D., & Engelman, D. M. (1992) *Proc. Natl. Acad. Sci. U.S.A. 89*, 748−752.
Flanagan, J. M., Kataoka, M., Fujisawa, T., & Engelman, D. M. (1993) *Biochemistry 32*, 10359−10370.
Galley, W. C., & Purkey, R. M. (1970) *Proc. Natl. Acad. Sci. U.S.A. 67*, 1116−1121.
Gittis, A. G., Stites, W. E., & Lattman, E. E. (1993) *J. Mol. Biol. 232*, 718−724.
Griko, Y. V., Privalov, P. L., Sturtevant, J. M., & Venyaminov, S. Y. (1988) *Proc. Natl. Acad. Sci. U.S.A. 85*, 3343−3347.
Grinvald, A., & Steinberg, I. Z. (1976) *Biochim. Biophys. Acta 27*, 663−678.
Hershberger, M. V., Maki, A. H., & Galley, W. C. (1980) *Biochemistry 19*, 2204−2209.
Hynes, T. R., Kautz, R. A., Goodman, M. A., Gill, J. F., & Fox, R. O. (1989) *Nature 339*, 73−76.
Johnson, M. L., & Fraiser, S. G. (1985) *Methods Enzymol. 117*, 301−342.
Kuwajima, K. (1989) *Proteins: Struct., Funct., Genet. 6*, 87−103.
Kuwajima, K. (1995) in *Methods in Molecular Biology, Vol. 40: Protein Stability & Folding: Theory & Practice* (Shirley, B. A., Ed.) pp 115−135, Humana Press Inc., Totowa, NJ.
Kwiram, A. L. (1982) in *Triplet State ODMR Spectroscopy* (Clarke, R. H., Ed.) pp 427−478, Wiley-Interscience, New York.
Lakowicz, J. R., Laczko, G., Gryczynski, I., & Cherek, H. (1986) *J. Biol. Chem. 261*, 2240−2245.
Lam, W.-C., Maki, A. H., Itoh, T., & Hakoshima, T. (1992) *Biochemistry 31*, 6756−6760.
Lipari, G., & Szabo, A. (1980) *Biophys. J. 30*, 489−506.
Loll, P., & Lattman, E. (1989) *Proteins: Struct., Funct., Genet. 5*, 183−201.
Lumry, R., Biltonen, R. L., & Brandts, J. F. (1966) *Biopolymers 4*, 917−944.
Maki, A. H. (1984) in *Biological Magnetic Resonance* Vol. 6, (Berliner, L. J., & Reuben, J., Eds.) Vol. 6, pp 187−293, Plenum Press, New York.
Myers, J. K., Pace, C. N., & Scholtz, J. M. (1995) *Protein Sci. 4*, 2138−2148.
Ramsay, G. D., & Eftink, M. R. (1994a) *Biophys. J. 31*, 516−523.
Ramsay, G. D., & Eftink, M. R. (1994b) *Methods Enzymol. 240*, 615−645.
Ramsay, G. D., Ionescu, R., & Eftink, M. R. (1995) *Biophys. J. 69*, 701−707.
Royer, C. A., Hincks, A. P., Loh, S. N., Prehoda, K. E., Peng, X., & Jonas, J. (1993) *Biochemistry 32*, 5222−5231.
Sreerama, N., & Woody, R. W. (1993) *Anal. Biochem. 209*, 32−44.
Shortle, D., & Meeker, A. K. (1986) *Proteins: Struct., Funct., Genet. 1*, 81−89.
Shortle, D., & Meeker, A. K. (1989) *Biochemistry 28*, 936−944.
Shortle, D., & Abeygunawardana, C. (1993) *Structure 1*, 121−134.
Shortle, D., Meeker, A., & Freire, E. (1988) *Biochemistry 27*, 4761−4768.
Shortle, D., Stites, W. E., & Meeker, A. K. (1990) *Biochemistry 29*, 8033−8041.
Sugawara, T., Kuwajima, K., & Sugai, S. (1991) *Biochemistry 30*, 2698−2706.
Tanaka, A., Flanagan, J., & Sturtevant, J. M. (1993) *Protein Sci. 2*, 567−576.
Wu, J. Q., Ozarowski, Z., & Maki, A. H. (1995) *J. Magn. Reson.* (in press)
Xie, D., Fox, R., & Freire, E. (1994) *Protein Sci. 3*, 2175−2184.

BI9530090